

Identifying hydrologic flowpaths on arctic hillslopes using electrical resistivity and self potential

Emily B. Voytek¹, Caitlin R. Rushlow², Sarah E. Godsey², and Kamini Singha³

ABSTRACT

Shallow subsurface flow is a dominant process controlling hillslope runoff generation, soil development, and solute reaction and transport. Despite their importance, the location and geometry of these flow paths are difficult to determine. In arctic environments, shallow subsurface flow paths are limited to a thin zone of seasonal thaw above permafrost, which is traditionally assumed to mimic the surface topography. We have used a combined approach of electrical resistivity tomography (ERT) and self-potential (SP) measurements to map shallow subsurface flow paths in and around water tracks, drainage features common to arctic hillslopes. ERT measurements delineate thawed zones in the subsurface that control flow paths, whereas SP is sensitive to groundwater flow. We have found that areas of low electrical resistivity in the water tracks were deeper than manual thaw depth estimates and varied from the surface topography. This finding suggests that traditional techniques might underestimate active-layer thaw and the extent of the flow path network on arctic hillslopes. SP measurements identify complex 3D flow paths in the thawed zone. Our results lay the groundwork for investigations into the seasonal dynamics, hydrologic connectivity, and climate sensitivity of spatially distributed flow path networks on arctic hillslopes.

INTRODUCTION

Water flow through the saturated soils of the shallow subsurface is often a dominant process controlling runoff generation (e.g., Hewlett and Hibbert, 1967), soil development (e.g., Lohse and

Dietrich, 2005), and solute transport (e.g., McGlynn and McDonnell, 2003) in watersheds. Despite their mechanistic importance, locating shallow subsurface flow paths remains challenging (Nippgen et al., 2015). Traditional methods for mapping shallow subsurface flow paths include direct observation through labor-intensive soil surveys and water content monitoring schemes (e.g., Tromp-van Meerveld and McDonnell, 2006; James and Roulet, 2007; Ali et al., 2011) or indirect predictions using terrain-based modeling (e.g., Jencso and McGlynn, 2011) or chemical or isotopic tracers (e.g., Tetzlaff et al., 2014). Direct and indirect methods have major drawbacks: tracer and modeling techniques are data intensive, and manual surveying is unsuitable for environments in which soil properties vary strongly through space or time.

In arctic systems, subsurface flow paths are limited in depth by the frozen boundary of permafrost (Woo, 2012). The soil profile is fully frozen in the winter, but higher energy inputs in the summer cause the progressive downward growth of a thawed subsurface region called the active layer, before the soils freeze again in the fall (e.g., Harris et al., 1988; Kane et al., 1991). The subsurface topography at the boundary between the thawed and frozen ground, which controls the location of shallow subsurface flow paths, is difficult to assess with direct observations over large regions, at a fine resolution, or through time (Nelson et al., 1998). Instead, subsurface topography is generally assumed to be a function of the surface topography (e.g., Stieglitz et al., 2003).

Geophysical techniques show promise for testing this assumption and mapping the active layer and subsurface flow paths on arctic hillslopes. Several techniques have been applied to permafrost systems, including electrical resistivity tomography (ERT), ground-penetrating radar, and electromagnetic (EM) methods (see the reviews by Scott et al., 1990; Kneisel et al., 2008; Hauck, 2013). Electrical methods are ideal for work in permafrost regions because bulk electrical resistivity depends on the temperature and phase of water (Ananyan, 1958; Hayley et al., 2007). Frozen ground is more resistive to electric current than is unfrozen ground, with typical

Manuscript received by the Editor 12 March 2015; revised manuscript received 17 July 2015; published online 29 January 2016.

¹Hydrologic Science and Engineering Program, Colorado School of Mines, Golden, Colorado, USA. E-mail: evoytek@mines.edu.

²Idaho State University, Department of Geoscience, Pocatello, Idaho, USA. E-mail: rushcait@isu.edu; godsey@isu.edu.

³Colorado School of Mines, Department of Geology and Geological Engineering, Colorado, USA and Hydrologic Science and Engineering Program, Colorado School of Mines, Golden, Colorado, USA. E-mail: ksingha@mines.edu.

© 2016 Society of Exploration Geophysicists. All rights reserved.

resistivity values more than 1000 ohm-m (Hauck and Kneisel, 2008), although the exact value varies depending on soil material and the proportional frozen/liquid water content (Ananyan, 1958). Recent theoretical calculations of resistivity changes due to temperature and water contents have been based on the variations of Archie's law, which relates bulk electrical conductivity to the fluid through porosity and empirically derived parameters (Hauck et al., 2011; Minsley et al., 2015). These relationships are the basis of using ERT to identify areas of partially frozen ground in the subsurface. ERT has previously been used to identify the frozen ground boundary in many settings in the continuous (Overduin et al., 2012) and discontinuous (Lewkowicz et al., 2011; McClymont et al., 2013) permafrost zones. Technological advances have also made long-term monitoring of permafrost boundaries possible, resulting in quantitative understanding of annual freeze-thaw cycles in mountain permafrost (e.g., Hauck, 2002; Hilbich et al., 2008; Krautblatter et al., 2010).

In addition to ERT and other active EM methods, self potential (SP) can help to inform our knowledge of subsurface processes in permafrost environments. SP is a passive electrical method that is sensitive to the small currents generated as water moves through soils. Voltage differences resulting from these currents are measured at the ground surface and analyzed to determine groundwater flow paths in the subsurface (e.g., Revil et al., 2005). The method has been used to successfully monitor hydrologic pumping tests (Rizzo et al., 2004; Jardani et al., 2009; Soueid Ahmed et al., 2014), identify flow through earthen dams (Ikard et al., 2014), and determine infiltration rates (Doussan et al., 2002; Suski et al., 2006). In periglacial environments, it has been used to investigate potential seepage through an ice-cored moraine (Moore et al., 2011). However, SP has not been previously used to identify subsurface flow paths in arctic hillslopes.

In this study, we pair ERT and SP to investigate groundwater flow paths in and around common drainage features of arctic hillslopes called water tracks. ERT images the basal boundary of the active layer, which controls shallow subsurface flow paths beneath water tracks on permafrost-underlain hillslopes, whereas SP maps the direction of groundwater flow through these features. We explore the direction and magnitude of flow beneath the primary channel of two water track features, and we investigate whether the subsurface topography mimics the surface topography along transects crossing the water tracks. Our study sets the stage for quantifying the seasonal growth, hydrologic connectivity, and climate sensitivity of spatially distributed flow path networks on arctic hillslopes.

FIELD SITE DESCRIPTION

In August 2014, a series of ERT profiles and SP data were collected in the Kuparuk River watershed of northern Alaska to characterize the thickness of an active-layer thaw (Figure 1). The watershed is underlain by continuous permafrost and defined locally by massive and gently sloping moraines of the Sagavanirktok River Glaciation (Hamilton, 1986). The ecology and hydrology of the Kuparuk River have been studied since the mid-1980s, and the river is currently part of the Arctic Long Term Ecologic Research site (e.g., Bowden et al., 2014). Six water tracks that drain into the Kuparuk River are extensively monitored as part of ongoing research. This study focuses on two water tracks, Water Tracks 1 and 6 (Figure 1), which were selected for their proximity to roads and to minimize interference with other experiments. High-

resolution topography from ground-based Light Detection and Ranging (LiDAR) collected during the same field campaign suggests that Water Track 1 drains 0.09 km² of hillslope at its weir on the western side of the river. Water Track 6 is approximately one-third the size of Water Track 1, draining 0.03 km² of the hillslope on the eastern side of the river. Both water tracks occur on the hillslopes with moist, acidic tundra vegetation, but the dominant emergent vegetation along the study reach of Water Track 1 is sedge, whereas Water Track 6 is characterized by abundant dwarf willows and birches. At both sites, a peaty organic soil horizon covers deeper mineral soils. The 24 soil cores collected at Water Track 1 in July and August 2014, 12 inside the water track feature and 12 outside on the nontrack hillslope, revealed that the organic soil horizon thickness was variable, but it was generally thicker inside the water track. The organic layer thickness inside Water Track 1 ranged from 23 to more than 88 cm, whereas the organic layer thickness outside the water track was usually less than 23 cm, ranging from only 3 to 43 cm in thickness. Some glacial erratics are visible on the surface at both sites, but organic soils cover >99% of the drainage area (Figure 2).

METHODS

Electrical resistivity tomography

ERT methods work by injecting electrical current into the ground using two electrodes and measuring the resulting voltage distribution at other electrode locations. From the known amount of injected current and measured voltage differences, a resistance can be calculated for each quadripole (combination of four electrodes). Multiple resistance measurements from different quadripole spacings and offsets can be combined through the process of inversion to produce a profile of subsurface resistivity. These methods have been used for delineating subsurface lithology and hydrologic units in a variety of settings (Pellerin, 2002; Robinson et al., 2008; see discussions in Parsekian et al., 2015). As discussed above, ERT has been used successfully in numerous permafrost settings to identify the extent of frozen ground.

ERT data were collected using an IRIS SyscalPro and stainless steel electrodes. Electrodes were inserted into the ground until good contact was made in the mineral soil or competent organic material, which was typically 10–15 cm below the land surface. Given the generally moist conditions, contact resistances between electrodes were low, with a median value of 4.1 and 6.5 kΩ between electrodes at Water Tracks 1 and 6, respectively. At both water tracks, ERT data were collected in a series of parallel transects, approximately centered on and perpendicular to, the primary drainage of the water track (Figure 1). One transect at each site was collected below a plywood weir installed for flow monitoring, whereas the remaining transects were collected upstream of the weir.

At Water Track 1, six parallel resistivity lines were collected approximately 20 m apart (Figure 1, Water Track 1). Each survey consisted of 96 electrodes at 0.5 m spacing, for a total transect length of 47.5 m. At Water Track 6, a similar collection scheme was used with a total of eight transects spaced 10 m apart (Figure 1, Water Track 6). Water Track 6 is narrower than Water Track 1, and therefore each ERT profile consisted of only 48 electrodes at 0.5 m spacing for a total of 23.5 m. Such fine spacing (0.5 m) was used to better capture the thaw boundary, which was estimated to be between 0.5 and 1 m below the ground surface from frost probing during August when

the geophysical data were collected. In August, the active layer thickness is nearly maximized for the year because the ground begins freezing again in September or early October.

Electrical resistivity tomography inversion

In ERT surveys, any combination of electrodes can be used for current injection and voltage measurements, but certain sequences have emerged that balance sensitivity and collection time. A dipole-dipole sequence was used for data collection at both sites due to its

speed and ability to detect lateral variations (Barker, 1979). At Water Track 1, the collection sequence for the 96-electrode transects included 1050 quadripoles, whereas 1159 quadripoles were used for the 48-electrode transects at Water Track 6. The collection sequence at Water Track 1 had fewer quadripoles despite the longer transect length because quadripoles sensitive to depths well below the permafrost boundary were not collected. Each quadripole was measured twice during a 500 ms current injection, and the relative error between the two measurements was used as a quality control and to weight the data during processing (median error = 0.1%).

Downloaded 02/04/16 to 138.67.24.11. Redistribution subject to SEG license or copyright; see Terms of Use at http://library.seg.org/

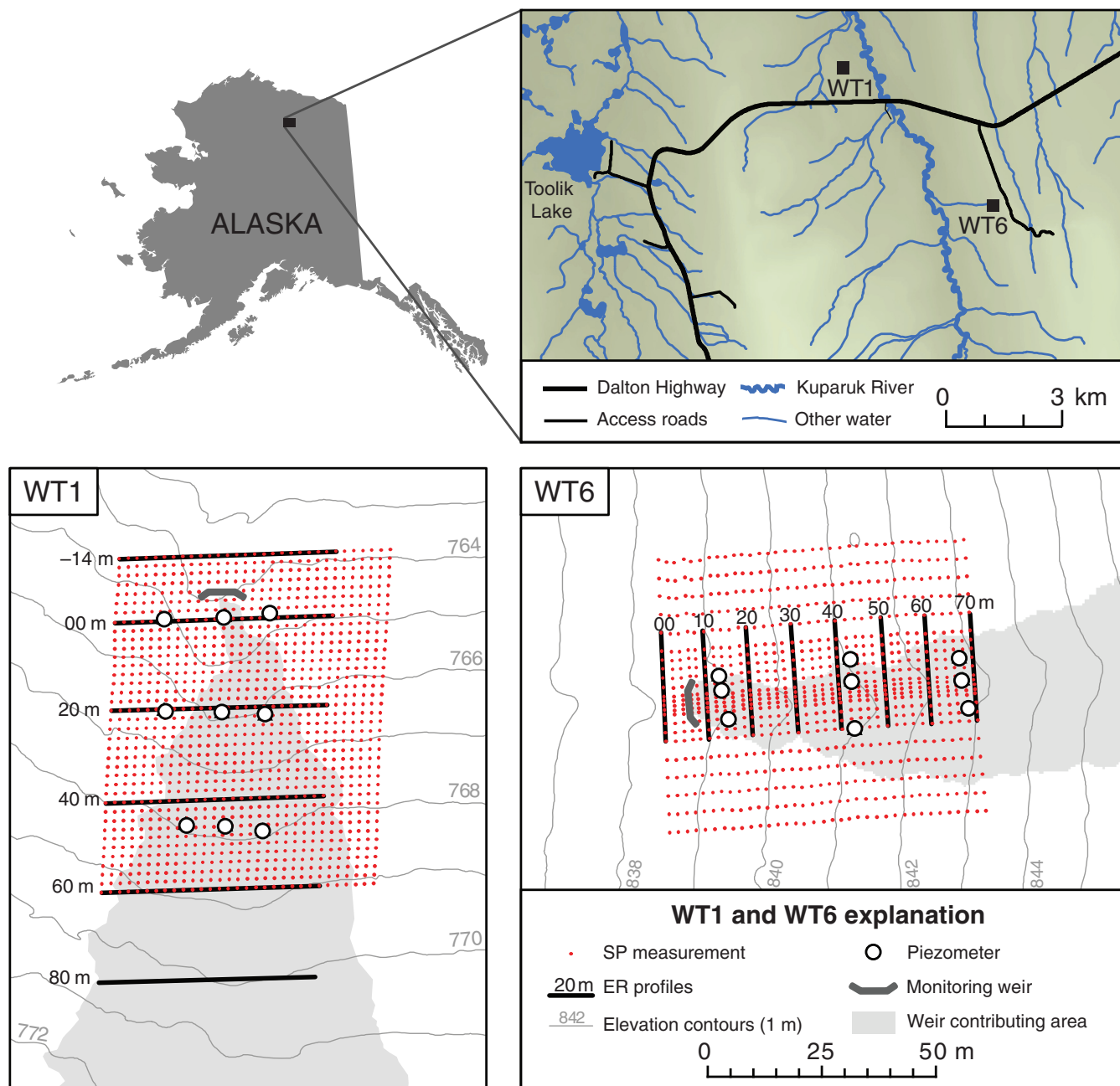


Figure 1. Regional map showing position of Water Tracks 1 and 6 relative to the Kuparuk River and the Dalton Highway (AK 11) in northern Alaska. Site maps of Water Tracks 1 and 6 showing the position of ERT transects relative to previously installed weirs and 2 m elevation contour intervals. The shaded areas represent the area contributing to flow at the monitoring weirs as calculated from ground-based LiDAR data.

The inversion code R2 was used to process the field data with a 0.125 m cell size; details of the code can be found in Binley and Kemna (2005). Each inversion converged in four to six iterations with an average root-mean-square error of 1.1 relative to the measured noise calculated by the stacking errors. The depth of investigation (DOI) method of Oldenburg and Li (1999) was used to determine what portion of the inverted profile was informed by the data, rather than the inversion parameters. This method involves processing the same data set at least two times, each regularized to different background resistivities. Areas that are informed by the data result in similar resistivity values in each of the two inversions;



Figure 2. Photo of Water Track 6 looking upslope from approximately 0 m ERT profile. The subtle topographic changes within the water track are highlighted by differences in vegetation. The weir, flume, and site-access boardwalks are in the foreground. The nine shallow groundwater wells are visible along the water track axis and on the adjacent nontrack hillslope.

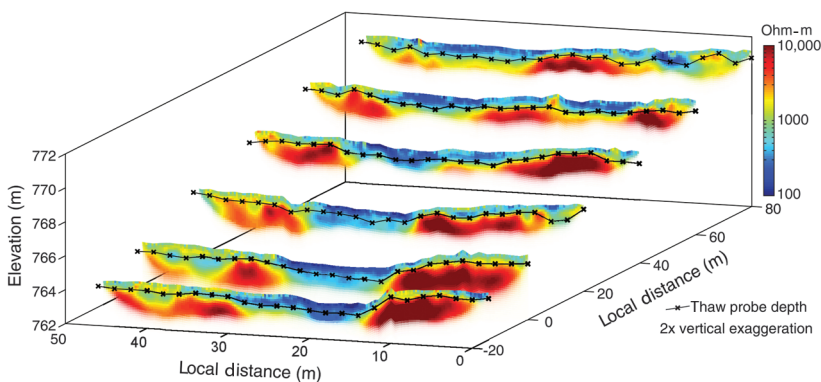


Figure 3. ERT profiles from Water Track 1 plotted on a local coordinate system. Elevations are shown in meters above sea level. Manual thaw probe data are indicated by black cross symbols. The vertical exaggeration is 2X.

areas beyond the DOI change as the background model is adjusted. These areas of lower data sensitivity are removed from plotting (Figures 3 and 4) to reduce the possibility of overinterpretation.

Self potential

SP is a passive geophysical technique that relies on measurements of voltage differences at the land surface. These voltage differences are created by naturally occurring electrical currents in the subsurface. One source of the electrical current is water flow through porous material or “streaming potential.” These currents initiate from the electrical double layer formed at the fluid-grain boundary (Revil and Leroy, 2001). As polar water molecules move past charged grain surfaces, a small electrical current is produced. The DOI for a passive technique, such as SP, is difficult to determine because it is dependent on the strength of the source, which is unknown.

At the water tracks, voltage differences between two Petiau-type (Petiau, 2000), nonpolarizing electrodes were measured with a Fluke 87 V handheld voltmeter. The reference electrode was buried approximately 20 cm to reduce drift caused by internal temperature variation. The temperature drift of Petiau-type electrodes is small, 0.22 mV/°C, relative to other nonpolarizing electrodes, which can exceed 2 mV/°C (Revil and Jardani, 2013). Individual measurements were collected in a grid using the roving electrode, typically placed on the surface or 0–3 cm into the ground when sediment allowed. The voltage difference between the reference and roving electrodes was checked every 60–120 measurements. The limited amount of drift between these electrodes observed during a survey (<3 mV), was assumed to be due to the temperature variations between the two electrodes, and it was distributed evenly over the intervening measurements during drift correction.

At Water Track 1, SP measurements were made in a 2-m grid across a 60 × 74 m area resulting in 1178 measurements. The measurement spacing at Water Track 6 was modified so that measurements were more densely spaced surrounding the primary channel (1-m spacing), and more widely spaced on the surrounding hillslopes (up to 4-m spacing) resulting in 828 measurements in a 60 × 70 m area. Due to spatial constraints, the footprints of the ERT and SP measurements are not identical at each of the sites, and their relative positions are shown in Figure 1.

To better evaluate the trends across each water track, a continuous surface was interpolated from the individual SP measurements (Figure 5). The surface was created by solving an inverse problem that minimizes the curvature of the surface, while respecting the confidence of the measurements.

The error was estimated by comparison of duplicate measurements made during the course of the SP surveys. The median error between repeat measurements at Water Tracks 1 and 6 was 1.5 mV. Because SP measurements are relative to the reference electrode, rather than absolute values, measured voltages at each water track have been shifted, so that the minimum value in each plot is zero.

Additional data sets

To compare the ERT-derived subsurface topography with surface topography, a 0.5 m digital elevation model for each site was generated using BCAL LiDAR tools (Boise Center Aerospace Laboratory, 2014) from point cloud data collected using a Riegl VZ-1000 scanner and retroreflective targets that were georeferenced with survey-grade GPS units. The precision of the point cloud collection and georeferencing was 3 cm or better. The LiDAR surveys were conducted over the same week in August 2014 as the geophysical investigations. Ground-surface elevation along the ERT profiles was also surveyed using an automatic level and stadia rod. At each survey location, the active-layer thickness (thaw depth) was measured as the refusal depth of a 3/8 in., hex-shaped, insulated steel frost probe inserted into the ground. Finally, at each site, a set of nine fully screened shallow groundwater wells outfitted with pressure transducers (Onset U20 sensors with a 3.7 m range) and referenced to an atmospheric pressure logger were used to monitor the depth to the water table. Three wells were installed along the channel of each water track, and a pair of wells was installed on either side of each water track well on the nontrack hillslope.

RESULTS AND DISCUSSION

Individual ERT profiles

The ERT profiles at both water tracks have a thin low-resistivity layer above a more resistive unit (Figures 3 and 4). This is the expected resistivity structure for a thin thawed layer over the frozen ground. At both sites, the low-resistivity layer is thicker within the water track compared with the nontrack hillslope. The thickening of the lower resistivity in the water track is due to enhanced thaw of the permafrost below the primary channel, which is also observed in the manual frost probe data. Enhanced thaw results from increased thermal conductivity due to higher water content (Hinzman et al., 1991; Yoshikawa et al., 2003) and snow insulation (Walker et al., 1999). Snow trapped in the topographic low within the water tracks leads to greater insulation from cold overwinter air temperatures and warmer soils. These processes also support the occurrence of the thickest low-resistivity zone directly upstream of the weir, where surface water ponding is continually present (weir position shown in Figure 1, thaw visible in the 0 m profile in Figure 3 and the 10 m profile in Figure 4).

The absolute resistivity values within these channels are lower than that of the lower resistivity values of the surrounding hillslopes. This trend is likely due to the differences in water content because increased water content would lower the bulk resistivity. Ponded water occurs on the surface upstream of the weirs at both

the water tracks. The shallow groundwater wells corroborate these general observations at their particular locations. The water table remained 4–8 cm above the ground surface at all three water track wells at Water Track 1 over the study period, whereas five of the six nontrack wells had water tables at depths ranging from 0 to 20 cm below the surface, with three wells with water tables at least 10 cm below the ground. Similar conditions were observed at Water Track 6, where two of the three water track wells had water tables above the ground surface throughout the study period, and the third had a fairly shallow water table, at depths of 3–7 cm. All nontrack wells at Water Track 6 recorded subsurface water tables 3–20 cm below ground surface. Water Track 6 shows a similar resistivity structure to Water Track 1, including a lower resistivity layer above a continuous high-resistivity layer (Figures 3 and 4). A secondary thawed path is also visible on the left side of the ERT of Figure 4. Neither secondary channel is visible in the surveyed elevation data, but they do appear in the higher resolution LiDAR data.

Manual frost probe measurements made every 2 m along each ERT transect suggest that the geometry of the base of the active layer is similar to that of the surface elevation. There is a slight deepening within the water tracks, relative to the surrounding non-track hillslopes (Figures 3 and 4), although the contrast is not as great as in the ERT data. Frost probe measurements were at times limited by the presence of boulders buried in the subsurface that prevented accurate identification of the base of the active layer. In these cases, measurements were made up to 0.5 m off the survey line, possibly resulting in the differences between the frost probe and ER data observed in Figure 6. The correlation between the ERT and frost probe boundaries is best outside of the main flow path (black cross symbols in Figures 3 and 4). A comparison of all four data types is shown in Figure 6. The ERT profiles also reveal areas of possible water movement that would not be detectable from frost probing alone. For example, it is impossible to accurately measure thaw depth below rocks using a frost probe. The ERT data revealed a large area of thaw beneath a rock that might facilitate water movement (Figure 3, 80 m transect at approximately 5 m across the transect). Rocks may transfer heat more effectively to the subsurface, especially during the snowmelt when their dark, lower albedo surfaces are exposed, enhancing permafrost thaw below.

A second previously unidentified area of thaw is in the low-resistivity bulb that occurs below the main flow path of the water

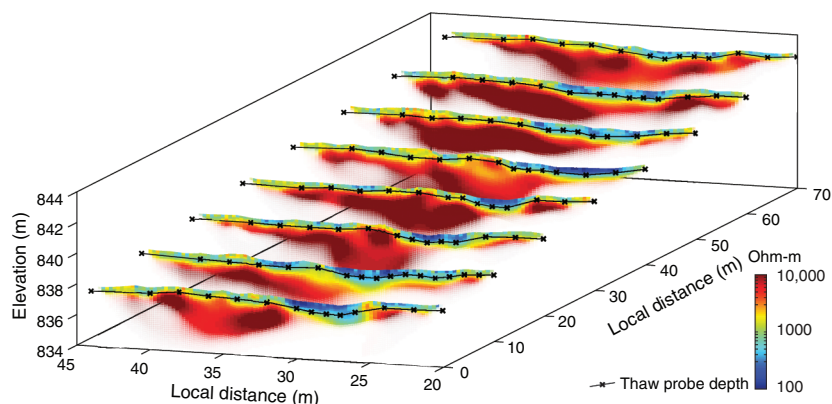


Figure 4. ERT profiles from Water Track 6 plotted on a local coordinate system. Elevations are shown in meters above sea level. Manual thaw probe data are indicated by black cross symbols. There is no vertical exaggeration.

track, particularly at Water Track 1, where the zone of low resistivity extends significantly deeper than is detected by the thaw probe. If the bulb areas were entirely thawed, it would be penetrable by a frost probe. If frozen, the resistivity would be similar to the surrounding frozen areas. Instead, the presence of a lower resistivity zone beyond the probe-observed frost boundary may indicate an area of partial thaw, in which the unfrozen water content is greater than surrounding areas at the depth. Individual ERT profiles cannot identify the water movement through the subsurface, but the lower resistivities suggest that liquid water may be present in these regions. It was not possible to sample these materials to make a conclusive interpretation of the origin of the lower resistivity materials. These data suggest that estimates of active layer thaw from manual frost-probe measurements underestimate the extent of potential flow in the subsurface and therefore the degree of hydrologic exchange between surface and subsurface water of arctic hillslopes.

Self-potential data

SP signals observed at the surface are a 2D rendering of complex 3D patterns in the subsurface. In purely horizontal flow, measured SP voltages should increase in the direction of flow (Revil and Jardani, 2013); flow paths down the hillslope should lead to increasing voltages downstream. In reality, observed signals are complex due to the superposition of multiple signal sources including horizontal and vertical components of flow paths and changes in ground resistivity. In Water Track 6 (Figure 5), values increase from 4 to 14 mV (yellow-green to blue) down the length of the primary

channel; this pattern is present but less obvious in Water Track 1. However, the SP signal does not increase monotonically in either data set. Instead, local maxima are present, likely due to groundwater contributions from the adjacent nontrack hillslope watershed into the primary channel. Since upward flow, as well as horizontal flow, can result in positive SP signals (Richards et al., 2010), these local maxima may also represent areas of local upwelling. These type of local maxima have been observed in the SP measurements in association with preferential flow paths through earthen dams (Bolève et al., 2009) and along faults (Richards et al., 2010). The inverse, local minima, have been observed associated with pumping wells (Rizzo et al., 2004).

We interpret the troughs in voltage on either side of the water tracks as hydrologic divides from which water is flowing away. This is supported by increasing voltage values in the lower left and right corners of Figure 5 (Water Tracks 1 and 6), suggesting that flow at these locations is moving toward the neighboring water track on the hillslope. These divides correspond approximately to the highs in both the surface topography from LiDAR (thick dashed lines in Figure 5), suggesting that at least on a broad scale, subsurface flow paths approximate surface patterns. Given the interprofile spacing (10–20 m), it is not possible to accurately compare divides derived from the ER data. However, the local minima occur in two locations where local upwelling might be expected: around the weir and in areas where the observed low-resistivity layer thins, forcing water through a thinner active layer. Around the weir, horizontal flow is blocked by an impermeable barrier, and therefore vertical water movement is expected.

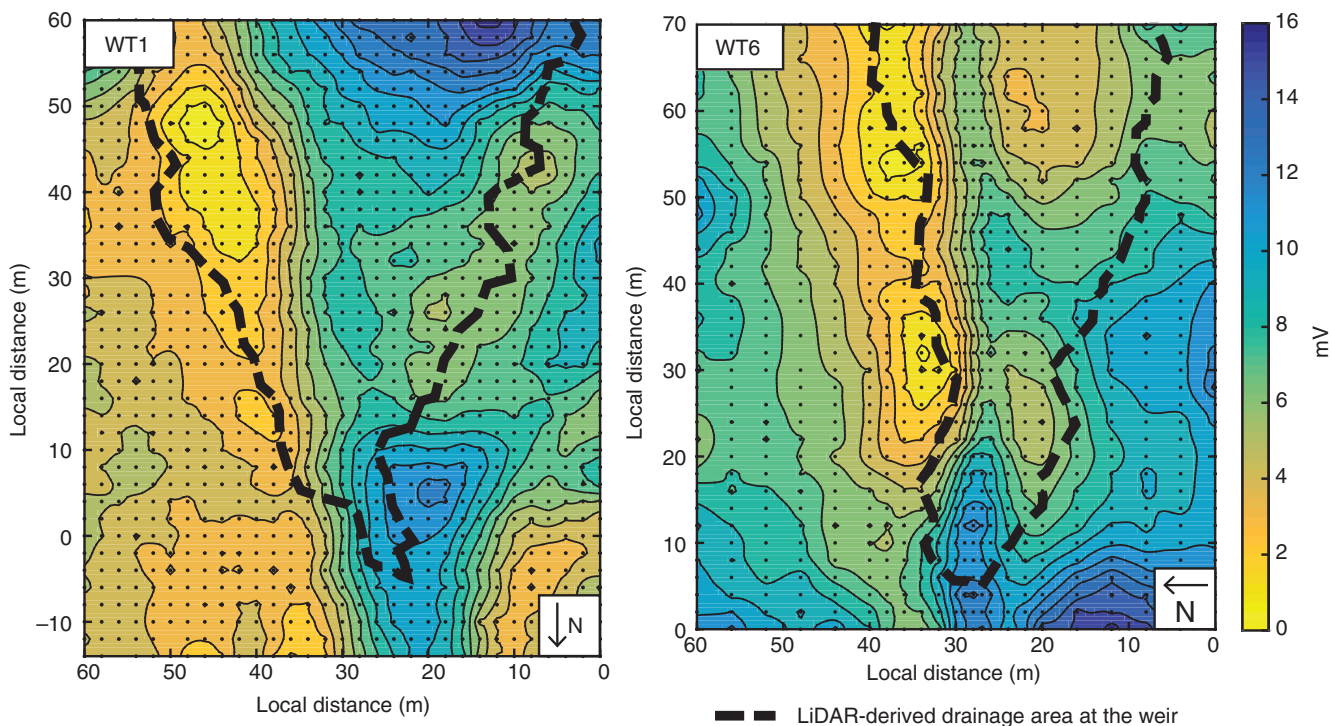


Figure 5. Plots of measured SP voltages. Measurement locations used in contour generation are shown as black dots. Surface contours are 2 mV. Yellow troughs are interpreted as hydrologic divides in the subsurface, with flow toward higher values (blue). LiDAR-derived drainage area at the weir is shown in thick dashed line for comparison.

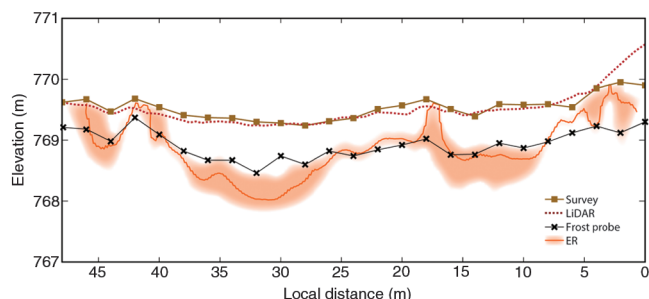


Figure 6. Comparison of the four types of data evaluated in the accumulation plots. Data shown are from the 60 m transect of Water Track 1. Surveyed elevation points are shown as brown squares, LiDAR-derived elevations are in red dashes, and the frost probe shown is as black cross symbols. The ER contour was selected using the mean of calculated resistivity values at each of the frost probe terminations. The cloud around the ER contour approximates one standard deviation from the mean value used to define the thaw depth. The deviations between LiDAR and surveyed elevations at edges are likely artifacts. Differences between frost probe and ER measurements may be due to the presence of shallow rocks, which forced frost probe measurements off the ER line.

An alternative source of voltage differences in SP data is changes in subsurface resistivity; however, in this case, the ground resistivity decreases from the flanks to the primary flow path. This direction of increasing resistivity would dampen, rather than enhance, the strength of the observed voltage differences (Revil and Jardani, 2013). Therefore, this suggests that the distribution of voltages we observe are primarily due to groundwater flow rather than changes in resistivity.

CONCLUSION

We compared measurements of active-layer thaw beneath common arctic hillslope drainage features called water tracks using ERT and depth-to-refusal frost probing. Frost probe and ERT data compared well in the areas of moist acidic tundra on the hillslope outside the water tracks, but in the water tracks, zones of lower electrical resistivity extend deeper than the frost probe measurements. These areas below the main water track flow path may represent partially frozen, saturated soil, an extension of the flow path network that is not identifiable with traditional methods. Future work should focus on using ERT to better resolve the interannual active layer thaw response to variable energy and water inputs. In particular, ERT could be a valuable tool for long-term mapping and prediction of the response of terrestrial flow path networks in permafrost regions to climate change.

The SP data indicate that on a hillslope scale, flow paths generally follow the surface topography. However, on a smaller scale, the SP measurements do not increase monotonically as would be expected from purely lateral flow. SP voltages increase along and toward the primary channel, suggesting flow toward the channel and downhill; however, local maxima are present within the water track, which could result from local upwelling. Incorporation of this type of data could lead to more targeted sampling to identify potential hotspots for biogeochemical transformation. SP could also be used to investigate how water flow changes through time; together with ERT, these data provide insight on how flow paths and the frost boundary interrelate.

ACKNOWLEDGMENTS

Financial support for this work was provided by National Science Foundation Office of Polar Programs (award no.: 1259930). Logistical support was provided by CH2M Hill Polar Services and the staff of Toolik Field Station. Terrestrial LiDAR support was provided by UNAVCO. We thank A. Revil and B. Minsley for conversations about the SP data collection and interpretation, and F. Day-Lewis for help to contouring the SP surfaces. Additional support was provided by the Department of Defense through the National Defense Science & Engineering Graduate Fellowship to E. B. Voytek.

REFERENCES

- Ali, G. A., C. L'Heureux, A. G. Roy, M. C. Turmel, and F. Courchesne, 2011, Linking spatial patterns of perched groundwater storage and storm-flow generation processes in a headwater forested catchment: *Hydrological Processes*, **25**, 3843–3857, doi: [10.1002/hyp.v25.2510.1002/hyp.v25.25](https://doi.org/10.1002/hyp.v25.2510.1002/hyp.v25.25).
- Ananyan, A. A., 1958, Dependence of electrical conductivity of frozen rocks on moisture contents: *Bulletin of the Academy of Science USSR*, **12**, 878–881.
- Barker, R.D., 1979, Signal contributions sections and their use in resistivity studies: *Geophysical Journal International*, **59**, 123–129, doi: [10.1111/j.1365-246X.1979.tb02555.x](https://doi.org/10.1111/j.1365-246X.1979.tb02555.x).
- Binley, A., and A. Kemna, 2005, DC resistivity and induced polarization methods, in Y. Rubin, and S. S. Hubbard, eds., *Hydrogeophysics*: Springer, 129–156.
- Boise Center Aerospace Laboratory, 2014, BCAL LiDAR Tools, <https://bcal.boisestate.edu/tools/lidar/>, accessed 1 November 2014.
- Bolève, A., A. Revil, F. Janod, J. L. Mattiuzzo, and J. J. Fry, 2009, Preferential fluid flow pathways in embankment dams imaged by self-potential tomography: *Near Surface Geophysics*, **7**, 447–462, doi: [10.3997/1873-0604.2009012](https://doi.org/10.3997/1873-0604.2009012).
- Bowden, W. B., B. J. Peterson, L. A. Deegan, A. D. Huryn, J. P. Benstead, H. Golden, M. Kendrick, S. M. Parker, E. Schuett, J. Vallino, and J. E. Hobbie, 2014, Ecology of streams of the Toolik region, in J. E. Hobbie, B. J. Peterson, and G. W. Kling, eds., *Alaska's changing Arctic: Ecological consequences for tundra, streams, and lakes*. Part of the Long-term Ecological Research Network research synthesis series: Oxford University Press, 173–237.
- Doussan, C., L. Jouniaux, and J. L. Thony, 2002, Variations of self-potential and unsaturated water flow with time in sandy loam and clay loam soils: *Journal of Hydrology*, **267**, 173–185, doi: [10.1016/S0022-1694\(02\)00148-8](https://doi.org/10.1016/S0022-1694(02)00148-8).
- Hamilton, T. D., 1986, Late Cenozoic glaciation of the central Brooks range, in T. D. Hamilton, K. M. Reed, and R. M. Thorson, eds., *Glaciation in Alaska: The geologic record*: Alaska Geological Society, 9–50.
- Harris, S.A., H.M. French, J.A. Heginbottom, G.H. Johnston, B. Ladanyi, D.C. Sego, and R.O. van Everdign, 1988, *Glossary of permafrost and related ground-ice terms*: National Research Council of Canada.
- Hauck, C., M. Böttcher, and H. Maurer, 2011, A new model for estimating subsurface ice content based on combined electrical and seismic data sets: *The Cryosphere*, **5**, 453–468, doi: [10.5194/tc-5-453-2011](https://doi.org/10.5194/tc-5-453-2011).
- Hauck, C., 2002, Frozen ground monitoring using DC resistivity tomography: *Geophysical Research Letters*, **29**, 1–4, doi: [10.1029/2002GL014995](https://doi.org/10.1029/2002GL014995).
- Hauck, C., 2013, New concepts in geophysical surveying and data interpretation for permafrost terrain: *Permafrost and Periglacial Processes*, **24**, 131–137, doi: [10.1002/ppp.1774](https://doi.org/10.1002/ppp.1774).
- Hauck, C., and C. Kneisel, 2008, *Applied geophysics in periglacial environments*: Cambridge University Press.
- Hayley, K., L. R. Bentley, M. Gharibi, and M. Nightingale, 2007, Low temperature dependence of electrical resistivity: Implications for near surface geophysical monitoring: *Geophysical Research Letters*, **34**, L18402, doi: [10.1029/2007GL031124](https://doi.org/10.1029/2007GL031124).
- Hewlett, J. D., and A. R. Hibbert, 1967, Factors affecting the response of small watershed to precipitation in humid areas: *Forest Hydrology*, 275–290.
- Hilbich, C., C. Hauck, M. Hoelzle, M. Scherler, L. Schudel, I. Völksch, D. Vonder Mühl, and R. Mäusbacher, 2008, Monitoring mountain permafrost evolution using electrical resistivity tomography: A 7-year study of seasonal, annual, and long-term variations at Schilthorn, Swiss Alps: *Journal of Geophysical Research*, **113**, 1–12, doi: [10.1029/2007JF000799](https://doi.org/10.1029/2007JF000799).
- Hinzman, L. D., D. L. Kane, R. E. Gieck, and K. R. Everett, 1991, Hydrologic and thermal properties of the active layer in the Alaskan Arctic: *Cold*

- Regions Science and Technology, **19**, 95–110, doi: [10.1016/0165-232X\(91\)90001-W](https://doi.org/10.1016/0165-232X(91)90001-W).
- Ikard, S. J., A. Revil, M. Schmutz, M. Karaoulis, A. Jardani, and M. Mooney, 2014, Characterization of focused seepage through an earthfill dam using geoelectrical methods: *Groundwater*, **52**, 952–965, doi: [10.1111/gwat.2014.52](https://doi.org/10.1111/gwat.2014.52).
- James, A. L., and N. T. Roulet, 2007, Investigating hydrologic connectivity and its association with threshold change in runoff response in a temperate forested watershed: *Hydrological Processes*, **21**, 3391–3408, doi: [10.1002/hyp.6554](https://doi.org/10.1002/hyp.6554).
- Jardani, A., A. Revil, W. Barrash, A. Crespy, E. Rizzo, S. Straface, M. Cardiff, B. Malama, C. Miller, and T. Johnson, 2009, Reconstruction of the water table from self-potential data: A Bayesian approach: *Groundwater*, **47**, 213–227, doi: [10.1111/gwat.2009.47.issue-2](https://doi.org/10.1111/gwat.2009.47.issue-2).
- Jencso, K. G., and B. L. McGlynn, 2011, Hierarchical controls on runoff generation: Topographically driven hydrologic connectivity, geology, and vegetation: *Water Resources Research*, **47**, W11527, doi: [10.1029/2011WR010666](https://doi.org/10.1029/2011WR010666).
- Kane, D. L., L. D. Hinzman, and J. P. Zurling, 1991, Thermal response of the active layer to climatic warming in a permafrost environment: *Cold Regions Science and Technology*, **19**, 111–122, doi: [10.1016/0165-232X\(91\)90002-X](https://doi.org/10.1016/0165-232X(91)90002-X).
- Kneisel, C., C. Hauck, R. Fortier, and B. Moorman, 2008, Advances in geophysical methods for permafrost investigations: *Permafrost and Periglacial Processes*, **19**, 157–178, doi: [10.1002/\(ISSN\)1099-1530](https://doi.org/10.1002/(ISSN)1099-1530).
- Krautblatter, M., S. Verleysdonk, A. Flores-Orozco, and A. Kemna, 2010, Temperature-calibrated imaging of seasonal changes in permafrost rock walls by quantitative electrical resistivity tomography (Zugspitze, German/Austrian Alps): *Journal of Geophysical Research: Earth Surface*, **115**, 1–15, doi: [10.1029/2008JF001209](https://doi.org/10.1029/2008JF001209).
- Lewkowicz, A., B. Etzelmüller, and S. L. Smith, 2011, Characteristics of discontinuous permafrost based on ground temperature measurements and electrical resistivity tomography, Southern Yukon, Canada: *Permafrost and Periglacial Processes*, **22**, 320–342, doi: [10.1002/ppp.703](https://doi.org/10.1002/ppp.703).
- Lohse, K. A., and W. E. Dietrich, 2005, Contrasting effects of soil development on hydrological properties and flow paths: *Water Resources Research*, **41**, W12419, doi: [10.1029/2004WR003403](https://doi.org/10.1029/2004WR003403).
- McClymont, A., M. Hayashi, L. Bentley, and B. Christensen, 2013, Geophysical imaging and thermal modeling of subsurface morphology and thaw evolution of discontinuous permafrost: *Journal of Geophysical Research: Earth Surface*, **118**, 1826–1837.
- McGlynn, B. L., and J. J. McDonnell, 2003, Role of discrete landscape units in controlling catchment dissolved organic carbon dynamics: *Water Resources Research*, **39**, 1190, doi: [10.1029/2002WR001525](https://doi.org/10.1029/2002WR001525).
- Minsley, B. J., T. P. Wellman, M. A. Walvoord, and A. Revil, 2015, Sensitivity of airborne geophysical data to sublacustrine and near-surface permafrost thaw: *The Cryosphere*, **9**, 781–794, doi: [10.5194/tc-9-781-2015](https://doi.org/10.5194/tc-9-781-2015).
- Moore, J. R., A. Boleve, J. W. Sanders, and S. D. Glaser, 2011, Self-potential investigation of moraine dam seepage: *Journal of Applied Geophysics*, **74**, 277–286, doi: [10.1016/j.jappgeo.2011.06.014](https://doi.org/10.1016/j.jappgeo.2011.06.014).
- Nelson, F. E., K. M. Hinkel, N. I. Shiklomanov, G. R. Mueller, L. L. Miller, and D. A. Walker, 1998, Active-layer thickness in north central Alaska: Systematic sampling, scale, and spatial autocorrelation: *Journal of Geophysical Research*, **103**, 28963–28973, doi: [10.1029/98JD00534](https://doi.org/10.1029/98JD00534).
- Nippgen, F., B. L. McGlynn, and R. E. Emanuel, 2015, The spatial and temporal evolution of contributing areas: *Water Resources Research*, **51**, 4550–4573, doi: [10.1002/wrcr.v51.610.1002/wrcr.v51.6](https://doi.org/10.1002/wrcr.v51.610.1002/wrcr.v51.6).
- Oldenburg, D. W., and Y. Li, 1999, Estimating depth of investigation in DC resistivity and IP surveys: *Geophysics*, **64**, 403–416, doi: [10.1190/1.1444545](https://doi.org/10.1190/1.1444545).
- Overduin, P. P., S. Westermann, and K. Yoshikawa, 2012, Geoelectric observations of the degradation of nearshore submarine permafrost at Barrow (Alaskan Beaufort Sea): *Journal of Geophysical Research*, **117**: 1–9, doi: [10.1029/2011JF002088](https://doi.org/10.1029/2011JF002088).
- Parsekian, A. D., K. Singha, B. Minsley, W. S. Holbrook, and L. Slater, 2015, Multiscale geophysical imaging of the critical zone: *Reviews of Geophysics*, **53**, 1–26, doi: [10.1002/2014RG000465](https://doi.org/10.1002/2014RG000465).
- Pellerin, L., 2002, Applications of electrical and electromagnetic methods for environmental and geotechnical investigations: *Surveys in Geophysics*, **23**, 101–132, doi: [10.1023/A:1015044200567](https://doi.org/10.1023/A:1015044200567).
- Petiau, G., 2000, Second generation of lead-lead chloride electrodes for geophysical applications: *Pure and Applied Geophysics*, **157**, 357–382, doi: [10.1007/s000240050004](https://doi.org/10.1007/s000240050004).
- Revil, A., L. Cary, Q. Fan, A. Finizola, and F. Trolard, 2005, Self-potential signals associated with preferential ground water flow pathways in a buried paleo-channel: *Geophysical Research Letters*, **32**, 1–4, doi: [10.1029/2004GL022124](https://doi.org/10.1029/2004GL022124).
- Revil, A., and P. Leroy, 2001, Hydroelectric coupling in a clayey material: *Geophysical Research Letters*, **28**, 1643–1646, doi: [10.1029/2000GL012268](https://doi.org/10.1029/2000GL012268).
- Revil, A., and A. Jardani, 2013, *The self-potential method: Theory and applications in environmental geosciences*: Cambridge University Press.
- Richards, K., A. Revil, A. Jardani, F. Henderson, M. Batzle, and A. Haas, 2010, Pattern of shallow ground water flow at Mount Princeton Hot Springs, Colorado, using geoelectrical methods: *Journal of Volcanology and Geothermal Research*, **198**, 217–232, doi: [10.1016/j.jvolgeores.2010.09.001](https://doi.org/10.1016/j.jvolgeores.2010.09.001).
- Rizzo, E., B. Suski, A. Revil, S. Straface, and S. Troisi, 2004, Self-potential signals associated with pumping tests experiments: *Journal of Geophysical Research: Solid Earth*, **109**, 1–14, doi: [10.1029/2004JB003049](https://doi.org/10.1029/2004JB003049).
- Robinson, D. A., A. Binley, N. Crook, F. D. Day-Lewis, T. P. A. Ferre, V. J. S. Grauch, R. Knight, M. Knoll, V. Lakshmi, R. Miller, J. Nyquist, L. Pellerin, K. Singha, and L. Slater, 2008, Advancing process-based watershed hydrological research using near-surface geophysics: A vision for, and review of, electrical and magnetic geophysical methods: *Hydrological Processes*, **22**, 3604–3635.
- Scott, W., P. Sellmann, and J. Hunter, 1990, *Geophysics in the study of permafrost*, in S. Ward, ed., *Geotechnical and Environmental Geophysics*: SEG, 355–384.
- Soueid Ahmed, A., A. Jardani, A. Revil, and J. P. Dupont, 2014, Hydraulic conductivity field characterization from the joint inversion of hydraulic heads and self-potential data: *Water Resources Research*, **50**, 3502–3522, doi: [10.1002/2013WR014645](https://doi.org/10.1002/2013WR014645).
- Stieglitz, M., J. Shaman, J. P. McNamara, V. Engel, J. Shanley, and G. W. Kling, 2003, An approach to understanding hydrologic connectivity on the hillslope and the implications for nutrient transport: *Global Biogeochemical Cycles*, **17**, 1105, doi: [10.1029/2003GB002041](https://doi.org/10.1029/2003GB002041).
- Suski, B., A. Revil, K. Titov, P. Konosavsky, M. Voltz, C. Dagès, and O. Huttel, 2006, Monitoring of an infiltration experiment using the self-potential method: *Water Resources Research*, **42**, W08418, doi: [10.1029/2005WR004840](https://doi.org/10.1029/2005WR004840).
- Tetzlaff, D., C. Birkel, J. Dick, J. Geris, and C. Soulsby, 2014, Storage dynamics in hydrogeological units control hillslope connectivity, runoff generation, and the evolution of catchment transit time distributions: *Water Resources Research*, **50**, 969–985, doi: [10.1002/2013WR014147](https://doi.org/10.1002/2013WR014147).
- Tromp-van Meerveld, H. J., and J. J. McDonnell, 2006, Threshold relations in subsurface stormflow: Part 2: The fill and spill hypothesis: *Water Resources Research*, **42**, 1–11, doi: [10.1029/2004WR003800](https://doi.org/10.1029/2004WR003800).
- Walker, M. D., D. A. Walker, J. M. Welker, A. M. Arft, T. Bardsley, P. D. Brooks, J. T. Fahnestock, M. H. Jones, M. Losleben, A. N. Parsons, T. R. Seastedt, and P. L. Turner, 1999, Long-term experimental manipulation of winter snow regime and summer temperature in arctic and alpine Tundra: *Hydrological Processes*, **13**, 2315–2330, doi: [10.1002/\(ISSN\)1099-108510.1002/\(ISSN\)1099-1085](https://doi.org/10.1002/(ISSN)1099-108510.1002/(ISSN)1099-1085).
- Woo, M., 2012, *Permafrost hydrology*: Springer.
- Yoshikawa, K., W. R. Bolton, V. E. Romanovsky, M. Fukuda, and L. D. Hinzman, 2003, Impacts of wildfire on the permafrost in the boreal forests of Interior Alaska: *Journal of Geophysical Research*, **108**, 1–14, doi: [10.1029/2001JD000438](https://doi.org/10.1029/2001JD000438).